

Elsevier Editorial System(tm) for Wear of Materials 2011 Special Issue  
Manuscript Draft

Manuscript Number:

Title: Tribocorrosion Behavior of CoCrMo Alloy for Hip Prostheses as a function of Loads: A Comparison between Two Testing Systems

Article Type: Research Paper

Keywords: Tribocorrosion, CoCrMo alloy, Normal Load, Metallic Implants, Synergism

Corresponding Author: Dr Mathew Mathew, PhD

Corresponding Author's Institution:

First Author: MJ Runa, BS

Order of Authors: MJ Runa, BS; Mathew Mathew, PhD; M Laurent, PhD; J.J Jacobs, PhD; LA Rocha, PhD; MA Wimmer, PhD

Abstract: Metal-on-metal (MOM) hip prosthesis bearings have enjoyed renewed popularity, but concerns remain with wear debris and metal ion release causing a negative response in the surrounding tissues. Further understanding into the wear and corrosion mechanisms occurring in MOM hips is therefore essential.

The purpose of this study was to evaluate the tribocorrosion behaviour, or interplay between corrosion and wear, of a low-carbon CoCrMo alloy as a function of loading. The tribocorrosion tests were performed using two tribometer configurations. In the first configuration, "System A", a linearly reciprocating alumina ball slid against the metal flat immersed in a phosphate buffer solution (PBS). In the second configuration, "System B", the flat end of a cylindrical metal pin was pressed against an alumina ball that oscillated rotationally, using bovine calf serum (BCS) as the lubricant and electrolyte. System B was custom-built to emulate in vivo conditions.

The tribocorrosion tests were performed under potentiostatic conditions at  $-0.345$  V, with a sliding duration of 1800 seconds and a frequency of 1Hz. In System A, the applied loads were 0.05, 0.5, and 1 N, in System B, the applied loads were 16, 32, and 64 N (515, 650, and 815 MPa). Electrochemical impedance spectroscopy (EIS), the double layer capacitance and polarization resistance were estimated. The total mass loss ( $K_{wc}$ ) in the CoCrMo was determined. The mass loss due to wear ( $K_w$ ) and that due to corrosion ( $K_c$ ) were determined. The dominant wear regime for the CoCrMo alloy subjected to sliding changes from wear - corrosion to mechanical wear as the contact stress increases. An attempt was made to compare both system, in their tribochemical responses and formulate some insights in total degradation processes. Our results also suggest that the proteins in the serum lubricant assist in the generation of a protective layer against corrosion during sliding. The study highlights the need of adequate methodology/guidelines to compare the results from different test systems and translating in solving the practical problems

# Tribocorrosion Behavior of CoCrMo Alloy for Hip Prostheses as a function of Loads: A Comparison between Two Testing Systems

M.J. Runa<sup>1, 2</sup>, M.T. Mathew<sup>2</sup>, M. Laurent<sup>2</sup>, J.J. Jacobs<sup>2</sup>, L.A. Rocha<sup>1</sup>, M.A. Wimmer<sup>2</sup>

<sup>1</sup> Center for Mechanical and Materials Technologies (CT2M), Department of Mechanical Engineering, University of Minho, Azurém, 4800-058 Guimarães, Portugal.

<sup>2</sup> Section of Tribology, Department of Orthopedic Surgery, Rush University Medical Center, 60612 Chicago, IL, USA.

Received Date Line (to be inserted by Production) (8 pt)

---

## Abstract

Metal-on-metal (MOM) hip prosthesis bearings have enjoyed renewed popularity, but concerns remain with wear debris and metal ion release causing a negative response in the surrounding tissues. Further understanding into the wear and corrosion mechanisms occurring in MOM hips is therefore essential.

The purpose of this study was to evaluate the tribocorrosion behaviour, or interplay between corrosion and wear, of a low-carbon CoCrMo alloy as a function of loading. The tribocorrosion tests were performed using two tribometer configurations. In the first configuration, “System A”, a linearly reciprocating alumina ball slid against the metal flat immersed in a phosphate buffer solution (PBS). In the second configuration, “System B”, the flat end of a cylindrical metal pin was pressed against an alumina ball that oscillated rotationally, using bovine calf serum (BCS) as the lubricant and electrolyte. System B was custom-built to emulate *in vivo* conditions.

The tribocorrosion tests were performed under potentiostatic conditions at  $-0.345$  V, with a sliding duration of 1800 seconds and a frequency of 1Hz. In System A, the applied loads were 0.05, 0.5, and 1 N, in System B, the applied loads were 16, 32, and 64 N (515, 650, and 815 MPa). Electrochemical impedance spectroscopy (EIS), the double layer capacitance and polarization resistance were estimated. The total mass loss ( $K_{wc}$ ) in the CoCrMo was determined. The mass loss due to wear ( $K_w$ ) and that due to corrosion ( $K_c$ ) were determined. The dominant wear regime for the CoCrMo alloy subjected to sliding changes from wear – corrosion to mechanical wear as the contact stress increases. An attempt was made to compare both system, in their tribochemical responses and formulate some insights in total degradation processes. Our results also suggest that the proteins in the serum lubricant assist in the generation of a protective layer against corrosion during sliding. The study highlights the need of adequate methodologies/guidelines to compare the results from different test systems and translating in solving the practical problems

**Keywords:** Tribocorrosion, CoCrMo alloy, Normal Load, Metallic Implants, Synergism.

---

\*Corresponding author. Tel.: +1312-942-8310; fax: +1-312-942-4491  
E-mail address: [mathew\\_t\\_mathew@rush.edu](mailto:mathew_t_mathew@rush.edu) (M.T. Mathew)

## 1 **1. Introduction**

2 Metal-on-metal (MOM) bearings currently constitute about 35% of over 200,000  
3 primary total hip replacement procedures performed annually in the US, a number that is  
4 expected to approach 600,000 by 2030 [1,2]. However, there are increasing reports of adverse  
5 local tissue responses mediated by degradation products - metal ions and wear debris -  
6 generated by wear and corrosion of metal-on-metal total hip replacements and surface  
7 replacements [2]. These degradation products can cause hypersensitivity, toxicological risk to  
8 systemic and remote sites and periprosthetic bone resorption [3-5].

9 The great majority of MOM bearings are made of CoCrMo alloys. These alloys have  
10 been extensively used in biomaterials for joint replacement due to their wear and corrosion  
11 resistance. A protective chromium oxide film forms on the surface of the alloy that inhibits  
12 corrosion and the release of metal ions [6-7]. The degree of protection depends on the  
13 composition of the oxide film, which in turn depends on the body fluids [8]. On the bearing  
14 surfaces, there is in addition the synergistic effect of wear and corrosion, i.e., tribocorrosion,  
15 that can markedly increase material loss [9-11]. Thus, the total material loss can be much  
16 higher than the material loss due to pure corrosion, without the influence of wear, or the  
17 material loss due to wear in absence of corrosion [12]. According to Stack et al [13], the  
18 dominant regime for material loss in the system can be inferred from the value of the  $K_c/K_w$   
19 ratio, where  $K_c$  is the material loss due to corrosion, calculated with Faraday's law from the  
20 current measured during the test. A value in the range of 0.1 to 1 corresponds to a corrosion-  
21 enhanced wear mechanism, whereas lower values point to a mechanism dominated by  
22 mechanical wear, and values higher than 1 to a mechanism dominated by wear-enhanced  
23 corrosion or outright corrosion [13].

24 Although the corrosion resistance of CoCrMo alloys has been extensively investigated,  
25 little work has been performed to evaluate their tribocorrosion behavior. Yan et al. [6] found  
26 that load and articulation could increase the corrosion rate and metal ion release, mostly Co  
27 ions. They also observed that electrochemical methods can affect the protein adsorptions  
28 process, resulting in the transition of wear and corrosion mechanisms. Recently, it has also  
29 been determined that CoCrMo hip bearing surfaces undergo microstructural changes and  
30 chemical reactions with the joint environment during articulation that produce a mechanically  
31 mixed zone of nanocrystalline metal and organic constituents, referred to as a biotribolayer.

1 This layer appears to be critical to reducing wear and corrosion [14]. Triboelectrochemical  
2 studies have been performed using various sliding contact test configurations that include pin-  
3 on-disk, pin- or ball-on-flat, and ring-on-disk [15].

4 The purpose of this study was to evaluate the tribocorrosion behavior as a function of  
5 load for a low-carbon CoCrMo alloy by using two different test set-ups, one a linearly  
6 reciprocating ball-on-flat configuration and the other a custom-made pin-on-ball setup that  
7 more closely simulates the hip *in vivo* conditions. We also sought to contrast two distinct test  
8 configurations, and determine to what extent the simpler configuration matched the more  
9 complex *in vivo*-like configuration.

10

## 11 **2. Materials and Methods**

12

### 13 **2.1. Overview**

14 The experimental design for this study consisted of using two wear test configurations  
15 or tribosystems to determine the parameters related to the tribocorrosion of a low-carbon  
16 CoCr<sub>28</sub>Mo<sub>6</sub> alloy subjected to sliding against an alumina counterface. In the first configuration,  
17 “System A”, a linearly reciprocating alumina ball slid against the metal flat immersed in a  
18 phosphate buffer solution (PBS). In the second configuration, “System B”, the flat end of a  
19 cylindrical metal pin was pressed against an alumina ball that oscillated rotationally, using  
20 bovine calf serum as the lubricant and electrolyte. System B was custom-built to emulate *in*  
21 *vivo* conditions. In both systems, the test chamber doubled as an electrochemical cell, with the  
22 CoCrMo component as the working electrode. All the tribocorrosion tests were performed in  
23 triplicate (n = 3), to check reproducibility, under potentiostatic conditions at -0.345 V, with a  
24 sliding duration of 1800 seconds and a frequency of 1Hz. The main input variable was load. In  
25 System A, the applied loads were 0.05, 0.5, and 1 N (150, 320, and 410 MPa initial Hertzian  
26 contact stress), matching the loads generally used in such tribometer for tribo-corrosion  
27 studies. In addition, such low loads might assist in investigating the nature of the passive film.  
28 In System B, the applied loads were 16, 32, and 64 N (515, 650, and 815 MPa initial Hertzian  
29 contact stress). This corresponded to approximately 15, 30 and 60 MPa respectively after  
30 running-in, which matches the average contact pressure of 50 MPa in the normal hip joint  
31 during the daily activities [16-17]. The numerical output variables were the polarization

1 resistance, the total material loss ( $K_{wc}$ ), the loss due to mechanical wear ( $K_w$ ) and the loss due  
 2 to corrosion or “chemical wear” ( $K_c$ ). Details of the materials and wear test configurations and  
 3 conditions follow.

4

## 5 **2.2. The CoCrMo Specimens**

6 The CoCrMo specimens were machined from rods of a low-carbon CoCrMo wrought  
 7 alloy per the Alloy 1 specification in ASTM Standard F 1537-07. The rods originated from two  
 8 sources, but had almost identical elemental compositions and similar hardness (Table 1). The  
 9 specimens consisted of disks 20 mm in diameter and 3.67 mm thick for the ball-on-plate  
 10 system (System A) and 12 mm in diameter and 7 mm in thickness for the pin-on-ball system  
 11 (System B). The test surfaces were mechanically polished to a mirror finish ( $R_a = 1.57 \pm$   
 12  $0.07$  nm), cleaned with propanol in an ultrasonic bath, rinsed with distilled water, and dried  
 13 using warm air prior to testing.

14 **Table 1.** Source, Rockwell hardness, and elemental composition of the low-carbon wrought  
 15 CoCrMo alloy used in this study.

Samples	Source	Original Rod Diameter (mm)	Rockwell C Hardness	Chemical Composition (%wt)						
				C	Co	Cr	Mo	Si	Mn	Al
System A	SURGIVAL (Spain)	30	38	0.037	64.81	27.82	5.82	0.36	0.78	<0.02
System B	ALLVAC (USA)	29	42	0.034	64.96	27.56	5.70	0.38	0.60	<0.02

16

## 17 **2.3. The Electrolytes**

18 The electrolyte used for the ball-on-plate system was phosphate buffered solution  
 19 (PBS) whereas the electrolyte and lubricant used for the pin-on-ball system was bovine calf  
 20 serum (BCS, supplied by Invitrogen corporation), diluted with a buffered saline solution to  
 21 have a protein concentration of 30 g/l. Their compositions are given in Tables 2 and 3,

1 respectively. The pH of both electrolytes was adjusted to 7.6, to be comparable to the pH of  
2 human joint fluid (synovial fluid).

3  
4 **Table 2** – Chemical composition of PBS solution, used in System A.

NaCl (g/L)	KH <sub>2</sub> PO <sub>4</sub> (g/L)	KCl (g/L)	Na <sub>2</sub> HPO <sub>4</sub> (g/L)
8.18	0.14	0.22	1.42

5  
6 **Table 3** – Chemical composition of BCS solution, used in System B.

NaCl (g/L)	EDTA (g/L)	Tris (g/L)	Protein (g/L)
9	0.2	27	30

7  
8  
9 **2.4. Tribocorrosion Tests**

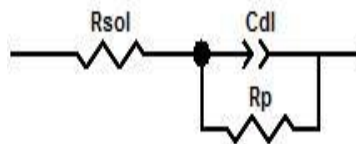
10 **2.4.1. Common Electrochemical Protocol**

11 The protocol for all the tribocorrosion tests entailed three phases: initial stabilization  
12 before the sliding test, the sliding test itself, and a final stabilization after the sliding test.  
13 Electrochemical impedance spectroscopy (EIS) measurements were performed using a  
14 potentiostat (Model Ref 600 (System A) and G300 (System B), Gamry Instruments,  
15 Warminster, PA, USA) before and after sliding. Using the *ZView* software (Scribner  
16 Associates, Southern Pines, NC, USA), the Randles EIS equivalent circuit (Fig.2) was used to  
17 determine the polarization resistance (Rp) and double layer capacitance (Cdl).

18 The applied anodic potential of -0.345V vs. SCE for the potentiostatic conditions was  
19 chosen based on the potentiodynamic curve from the initial corrosion tests (Figure 2) to  
20 represent a passive potential of the CoCrMo alloy in BCS and PBS. The corrosion potential,  
21  $E_{corr}$ , and the corrosion current density,  $I_{corr}$ , were obtained according to the Tafel's slope  
22 method and tabulated in the Figure 2. The changes from cathodic to anodic reactions occur at  
23 the corrosion potential ( $E_{corr}$ ). Above this potential the cathodic reactions are negligible and the  
24 current is determined by the kinetics of metal oxidation, the anodic reactions. A passive region  
25 can also be observed in both curves.

26

1

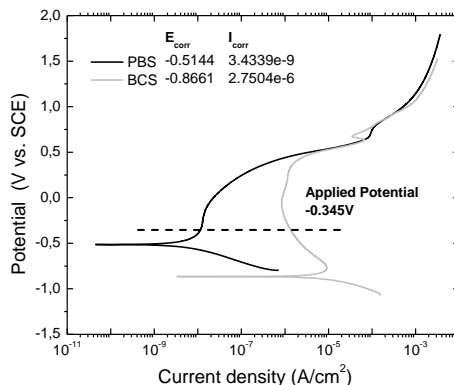


2

3

4

**Figure 1** Schematic diagram for the three-element Randles equivalent circuit used to determine the polarization resistance.



5

6

7

**Figure 2.** Polarization curve of low carbon CoCrMo alloy in PBS and BCS solutions. Potential range from -0.8 to 1.8V, scan rate of 1mV/sec.

8

9

### 2.4.2. The Tribometers

#### System A, Conventional CETR Tribometer

10

11

12

13

14

15

16

17

18

19

20

A CETR tribometer (Model UMT-2, CETR, Campbell, California, USA) was used in the ball-on-plate configuration, whereby a 10 mm diameter alumina ball slid against a CoCrMo disk in a linearly reciprocating path (Figure 3). The stroke length was 5 mm. A saturated calomel electrode (SCE) was used as the reference electrode (RE), a platinum (Pt) electrode as counter electrode (CE) and the CoCrMo disk as a working electrode (WE). The active area of the working electrode was 2.29 cm<sup>2</sup>. Tests were performed in two different electrochemically controlled techniques: (i) free potential condition (ii) potentiostatic test with an applied potential of -0.345V vs. SCE. Each test began with a cathodic cleaning treatment (potentiostatic condition at -0.8V vs. SCE) with the purpose to remove oxides that were air-formed at the surface. EIS measurements were carried out in a frequency range from 63kHz to

1 0.001Hz with 10 frequency/decades within. Each test was started with a fresh alumina ball  
 2 surface.

3 System B, Customized Tribosystem

4 This tribosystem entailed a pin-on-ball configuration in which the flat end of a  
 5 cylindrical CoCrMo pin was loaded against the equator of a rotationally oscillating 28 mm  
 6 diameter alumina ball (Figure 4). The oscillation frequency was 1Hz, with a ball rotation of  
 7  $\pm 15^\circ$  for 1800 cycles. A graphite rod was used as the counter electrode. The area of the sample  
 8 exposed to the electrolyte was  $1.13\text{cm}^2$ . Tests were also performed at  $E_{\text{corr}}$  and under  
 9 potentiostatic conditions with the same applied potential. The cleaning process was performed  
 10 at  $-0.9\text{V vs. SCE}$ . Electrochemical impedance was carried out in a frequency range from  
 11 100kHz to 0.005Hz, with 10 frequency/decades. Each test was started with a fresh alumina ball  
 12 surface. The test conditions and a comparison of tribometer Systems A and B are given in  
 13 Table 4.

14 Table 4 – Test conditions and a comparison between systems A and B.

Similarities		Differences	
		System A	System B
Applied potential	-0.345V	Pin-on-plate	Ball-on-flat
Sliding time	1800 sec	Reciprocating Motion	Oscillatory/rotary Motion
Number of cycles	1800		
Frequency	1Hz	Area exposed to electrolyte ( $2.28\text{ cm}^2$ )	Area exposed to electrolyte ( $1.13\text{ cm}^2$ )
Protocol	Three phases	Low loads (0.05N, 0.5N, 1N)	High loads (16N, 32N, 64N)
Material (sample)	LC-CoCrMo	PBS solution (30mL)	BCS solution (150mL)
Counterbody	Ceramic ball	Sliding distance-18m	Sliding distance-26.4 m
Average velocity		10 mm/s	14.7 mm/s
Velocity profile	Sinusoidal	Horizontal position of the plate causes the wear debris to spread in the vicinity of the contact zone	Vertical position of the pin causes the release of the wear debris to the solution (under gravity force)

15

16



1  
2  
3  
4  
5  
6  
7

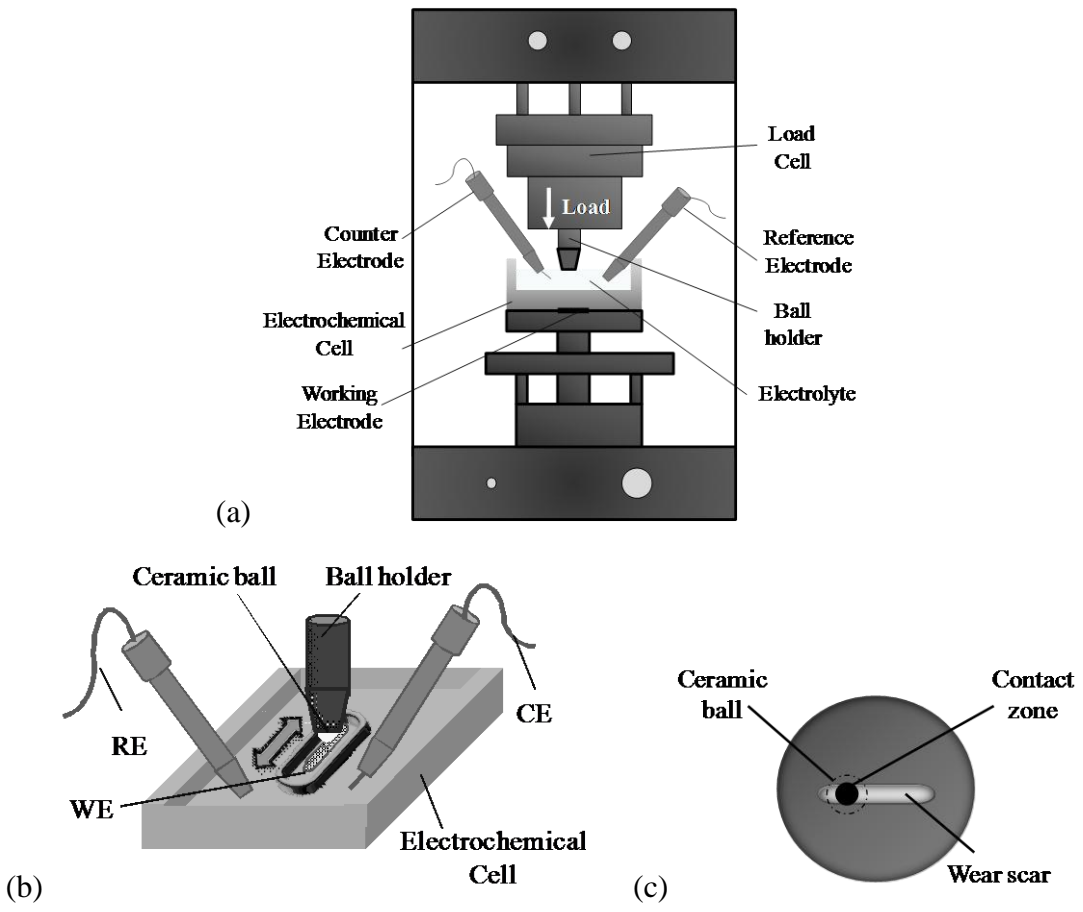
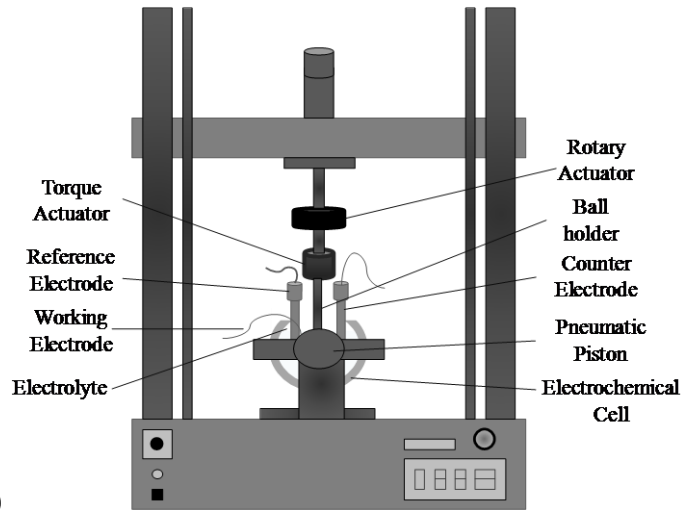


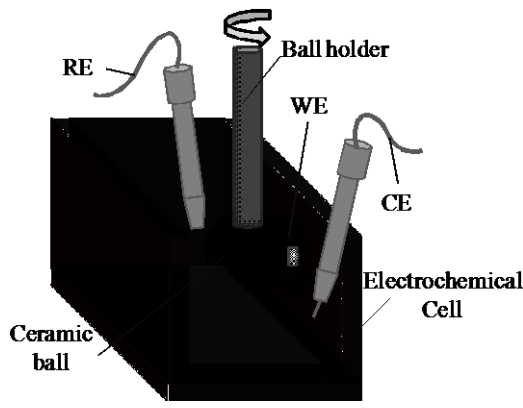
**Figure 3.** Depiction of the conventional CETR tribometer for System A. (a) Tribometer set-up. (b) Test area. (c) Top view of the test area. (WE = working electrode, CE = counter electrode RE = reference electrode.)

1

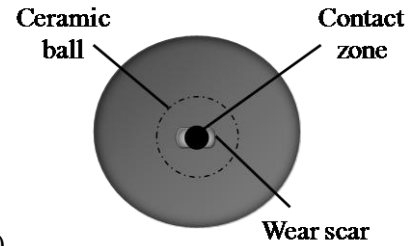


2

(a)



(b)



(c)

3

4

5 **Figure 4.** Depiction of the pin-on-ball custom built tribometer, System B, used in this study.

6 (a) The tribometer set-up. (b) The test area. (c) Top view of the test area. (WE = working

7 electrode, CE = counter electrode RE = reference electrode.)

8

9

10

## 2.5. Mass Loss Due to Wear and Corrosion

The total mass loss ( $K_{wc}$ ) during tribocorrosion is the sum of the loss due to wear ( $K_w$ ) and that due to corrosion ( $K_c$ ), so that [13]:

$$K_{wc} = K_w + K_c \quad (1)$$

To obtain  $K_w$ , topographical measurements of the wear scar were made using a scanning white light interferometry microscope (Zygo Corporation, Middlefield, CT, USA), from which the wear volume was calculated using the MetroPro 8 software (Zygo Corporation). The mass loss was then calculated by multiplying this volume by the density of the CoCrMo alloy,  $8.30 \text{ g/cm}^3$  [18].

The mass loss (g) due to corrosion was estimated from Faraday's equation

$$K_c = \frac{q \times M}{n \times F} \quad (2)$$

where  $q$  is the charge in coulombs passed through the working electrode,  $M$  (g/mole) is the atomic weight of the element being dissolved,  $n$  is the dissolution valence (in this study,  $n = 2$  was used for calculations) and  $F$  is Faraday's constant (96490 coulombs/mole). The charge  $q$  was calculated by integrating the current ( $i$ ) measured during the test over time ( $t$ ) (see Fig. 5).

## 2.6. Surface Characterization

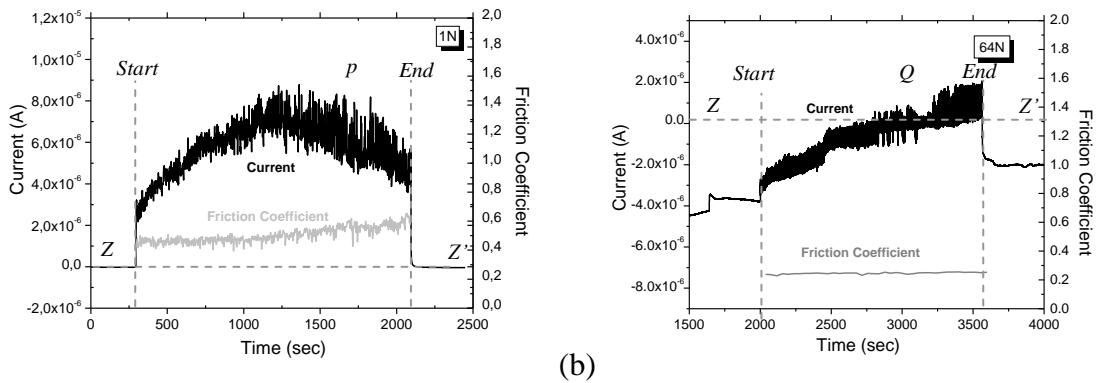
Morphological characterization of the surface was done using different techniques: Scanning Electron Microscopy (SEM) and Energy Dispersive x-ray Spectroscopy (EDS) (Model-Joel JSM-6490 LV, Oxford Instruments (England)), White Light interferometry (Zygo Corporation, Middlefield, CT, USA)

## 3. Results

### 3.1. Evolution of current and friction coefficient during the sliding test

During the tribocorrosion tests, the evolution of current and friction coefficient were monitored as a function of time are shown in Figure 5 for the maximum loads (1 N for System A and 64 N for System B). When the sliding started, the current abruptly increased to a higher value, corresponding to a sudden increase in the corrosion rate of the exposed surface as

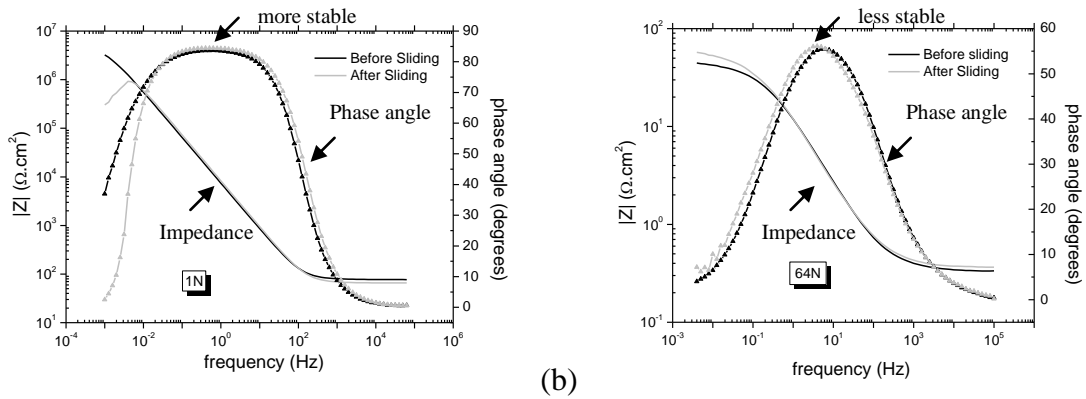
1 sliding removes the passive film and the surface left behind becomes unprotected. When  
 2 sliding stopped, the current decreased abruptly to a value similar to the initial one, as the metal  
 3 in the mechanically activated area repassivated. The oscillation of the current and friction  
 4 coefficient arise from the depassivation and repassivation of the metal surface, and follow the  
 5 cyclic motion (Figure 5). In addition, the test configuration and electrolyte influenced the  
 6 evolution of the current and friction coefficient. In System A, the current peaked midpoint in  
 7 time (Fig 5(a)), whereas in System B, the current gradually increased to more anodic values  
 8 throughout the test (Fig. 5(b)). The markedly higher friction coefficient in System A, compared  
 9 to System B..



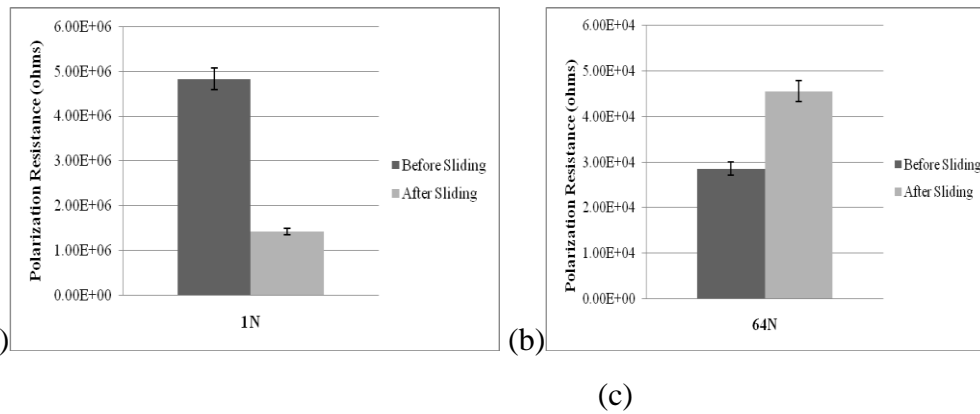
10 (a) (b)  
 11 **Figure 5** – Evolution of the current and the friction coefficient during a 30 minute sliding run  
 12 at (a) 1N in PBS solution (System A) and at (b) 64N in BCS solution (System B). Dotted line  
 13 (Z-Z') shows zero current.

### 14 3.2. Electrochemical impedance data before and after the sliding

15 The bode plots (impedance  $|Z|$  vs. frequency and phase angle vs. frequency) are  
 16 presented in Figure 6. For both solutions, only one time constant can be seen in the phase angle  
 17 (Figure 5, line with symbol) at lower frequencies. At the highest frequencies, the impedance  
 18 ( $|Z|$ ) and phase angle values tend to become constant, which is characteristic of resistive  
 19 behavior and arises from the electrolyte resistance [16-17]. It confirms the presence of a  
 20 compact, homogeneous and protective passive film on the surface. After sliding, the impedance  
 21 has decreased in System A (Figure 6(a), grey line, <0.01 Hz), whereas it has increased in  
 22 System B (Figure 6(b), grey line, <0.01 Hz). The increase denotes a slowing down of the  
 23 corrosion kinetics, possibly due to the presence of proteins in the BCS solution.



1 (a) (b)  
 2 **Figure 6** – Bode plot from electrochemical impedance spectroscopy measurements for (a) 1N  
 3 in PBS solution and for (b) 64N in BCS solution, System A and B, respectively.



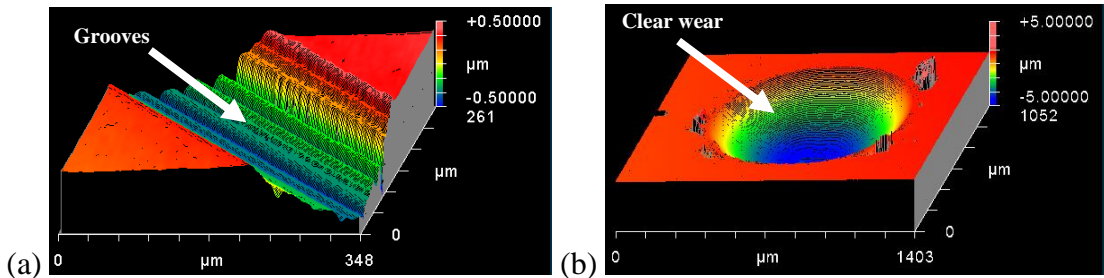
4  
 5 (a) (b)  
 6 (c)  
 7 **Figure 7** – Polarization resistance before and after sliding at the highest normal load in  
 8 System A (a) and in System B (b).

9 For all applied loads, the polarization resistance,  $R_p$ , was higher before sliding than after  
 10 sliding for System A, whereas the reverse was true for System B. This is shown graphically in  
 11 Figure 7 (a & b) for the highest load in each system. The low  $R_p$  after sliding indicates poor  
 12 corrosion resistance of the surface in System A (Figure 7 (a)), which might be due to the large  
 13 area of the worm surface (no passive film) and the presence of wear debris in the vicinity of the  
 14 contact zone. In contrast, the high  $R_p$  after sliding in System B indicates improved corrosion  
 15 resistance of the surface, perhaps connected to exposure to the proteins in solution. The  
 16 constant coverage of the worn area by the alumina counterface and the possibility for wear  
 17 debris to fall away might be other reasons for this observation.

1  
2  
3  
4  
5  
6  
7  
8  
9  
10

### 3.3. Wear scar profile and surface characterization

The wear scars shapes were consistent with the motion and shape of the alumina counterface. For System A, they were therefore grooves with an approximately circular arc cross-section (Figure 8(a)), whereas for System B, they consisted of an almost spherical depression (Figure 8(b)). In both cases, the wear volumes could be readily determined from topographical measurements. The corresponding weight losses are given in Table 5. The longitudinal scratches seen in the wear scars from System A may be associated with wear debris in the contact zone.

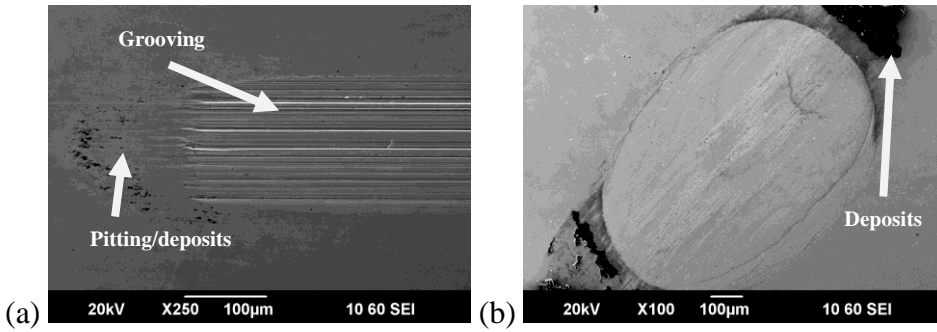


11  
12  
13  
14  
15  
16  
17  
18  
19  
20  
21  
22

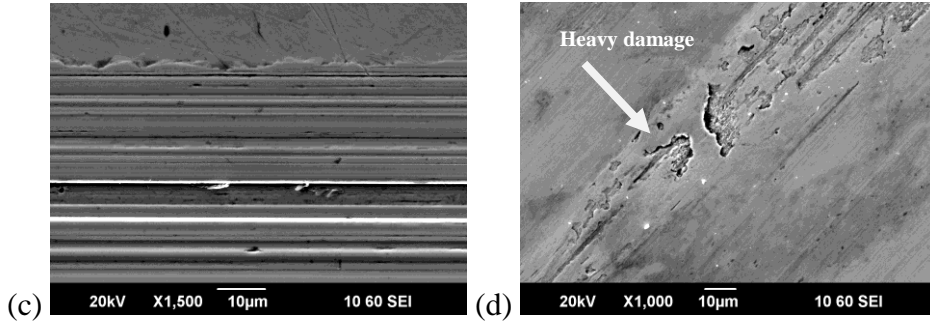
**Figure 8** - 3-dimensional image of the wear scar using Zygo Microscope, for (a) System A and (b) System B, with 1N and 64N, respectively.

Examination of the wear scars by SEM revealed some pitting corrosion at just beyond the motional ends of the wear scars (Figure 9(a) and 9(b)). These localized imperfections on the oxide layer were made by wear debris pushed to the edge where the movement stops. The debris damages the protective film, leading to pitting corrosion and corrosion products rich in oxygen as verified by EDS analysis (Figure 9(e)). Inside the wear track, wear debris particles were observed (Figure 9(c) and (d)), even though those surfaces had undergone cleaning in an ultrasonic bath prior to examination. These strongly adhering particles can induce current variations during the sliding [19].

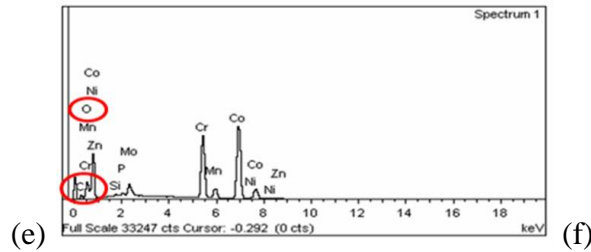
1



2



3



4 **Figure 9** – SEM micrographs of the wear scars on the CoCrMo surface for System A (left side,  
 5 a and b) at 1 N and System B (right side, c and d) at 64 N. A typical EDS spectrum for pits and  
 6 passive film on the surface (e).

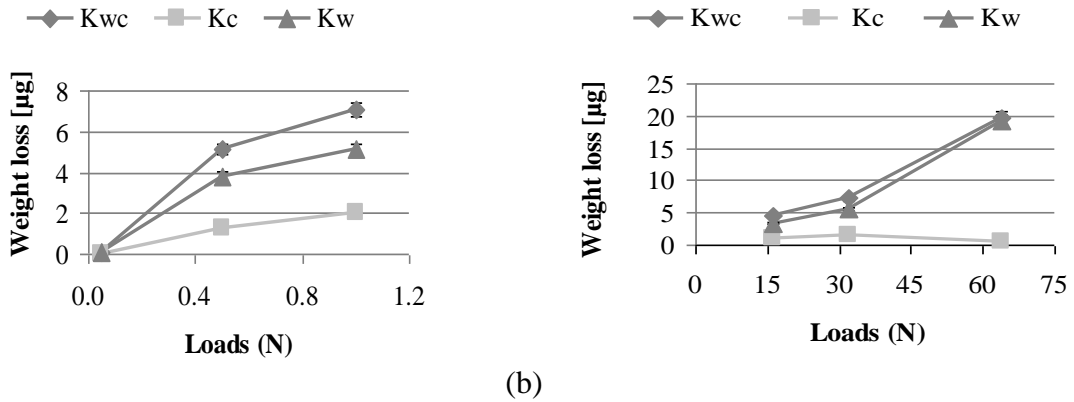
7 **3.4. Weight loss distribution as a function of load**

8 The weight loss distribution in terms of  $K_{wc}$  (total weight loss),  $K_c$  (weight loss due to  
 9 corrosion), and  $K_w$  (weight loss due to wear) as a function of load is shown graphically in  
 10 Figure 10 and tabulated in Table 5 for the both systems.

11 The total weight loss ( $K_{wc}$ ) and weight loss due to wear ( $K_w$ ) increase with load in both  
 12 systems. The weight loss due to corrosion increases with load for System A, but not for for  
 13 System B. The contribution of corrosion is consistently small compared with the contribution  
 14 of mechanical wear ( $K_{wc}$  and  $K_w$ , in Figure 10). Because metal loss due to corrosion is  
 15 estimated from the current measured during the tribocorrosion test, the influence of current

1 from the unworn area should not be neglected [19]. In this study, it is compensated by using  
 2 the current before sliding as the zero point.

3  
 4



5 (a) (b)  
 6 **Figure 10** – Total weight loss distribution for (a) System A and (b) System B.

7 **Table 5** – Wear-corrosion volume loss for the highest normal loads of both systems.

	Normal load	$K_{wc}$ [µg]	$K_w$ [µg]	$K_c$ [µg]	$K_c/K_w$
System A	0.05N	$0.08 \pm 0.12$	$0.07 \pm 0.10$	$0.01 \pm 0.02$	0.1981
	0.5N	$5.10 \pm 3.03$	$3.83 \pm 2.65$	$1.28 \pm 0.39$	0.3337
	1N	$7.09 \pm 7.65$	$5.10 \pm 8.06$	$2.00 \pm 0.43$	0.3916
System B	16N	$4.45 \pm 0.22$	$3.38 \pm 0.17$	$1.07 \pm 0.05$	0.3151
	32N	$7.25 \pm 0.36$	$5.62 \pm 0.28$	$1.63 \pm 0.08$	0.2891
	64N	$19.71 \pm 0.99$	$19.19 \pm 0.95$	$0.52 \pm 0.03$	0.0272

8

#### 9 **4. Discussion**

10 In this study we evaluated the tribocorrosion behavior of a low-carbon CoCrMo alloy,  
 11 using two test systems, namely, a conventional reciprocating sliding system (System A) and a  
 12 specially designed tribosystem emulating to some extent the hip joint contact conditions



1 (System B). System A is relevant from a practical point of view because it has been used by  
2 various research labs. We therefore also sought to contrast the two test configurations and  
3 determine to what extent the simpler configuration matched the more complex *in vivo*-like  
4 configuration, with an aim to capture the key test parameters for evaluating the tribocorrosion  
5 behavior of CoCrMo alloys used for joint bearings.

6 The markedly higher friction coefficient in System A (0.50) compared to System B  
7 (0.25) suggests that the proteins are acting as an effective boundary lubricant (see Fig. 5). The  
8 electrochemical impedance measurements indicate the presence of a compact, homogeneous  
9 and protective passive film on the surface for both systems. Evidence for this film is seen in  
10 SEM micrographs (Fig. 9). However, the increase after sliding of the impedance at low voltage  
11 excitation frequencies observed in System A (Fig. 6(a)) suggests the film that forms may offer  
12 less protection after sliding than before. The corresponding increase in impedance for System  
13 B (Fig. 6(b)) suggests the opposite, i.e., a more protective film after sliding than before. These  
14 impedance results are consistent with the trends observed for the polarization resistance,  $R_p$ . Its  
15 decrease after sliding for System A (Fig. 7 (a)) indicates decreased corrosion protection,  
16 whereas its increase for System B (Fig. 7 (b)) indicates increased protection. The latter is  
17 consistent with the formation of protective tribolayer.

18 The extent and shapes of the wear scars are indicative of the considerable difference in  
19 the motions and lubrication in the two systems. In System A, in which an alumina ball slides  
20 against a CoCrMo flat (Fig. 3), the horizontal reciprocating motion causes the oxide film on the  
21 metal to be constantly destroyed and re-formed. When the pin goes forward, it removes the  
22 protective film and the clean metal left behind can corrode more easily. It yields galvanic  
23 coupling of two distinct surface states of the metal: the passive metal (unworn area) and the  
24 bare metal (worn area) exposed to the solution by abrasion of the passive film. In System B, in  
25 which an alumina ball rotates back-and-forth against a CoCrMo flat (Fig. 4), the contact zone  
26 is a small, nearly circular area (Fig. 8 (b)) that restricts access of the electrolyte to corrode the  
27 unprotected surface [20-21].

28 In addition, the mechanical and electrochemical mechanisms during rubbing lead to the  
29 release of metallic wear particles, as observed in Figure 9(b & c). Those detached particles  
30 could form third bodies and be ejected from the contact, and/or be spread on the metal surface,  
31 resulting in the formation of solid oxides or dissolved ions. Thus, in System A there is the

1 accumulation of wear particles around the wear scar on the unworn area. Those small localized  
 2 particles will remove the protective film in that unworn area, inducing pitting corrosion,  
 3 increasing the size of the corroded area and the total amount of corrosion. On the other hand, in  
 4 System B the wear particles have a greater chance to disperse into the electrolyte under the  
 5 influence of gravity. [19, 22]

6 **4.1 Synergistic interactions**

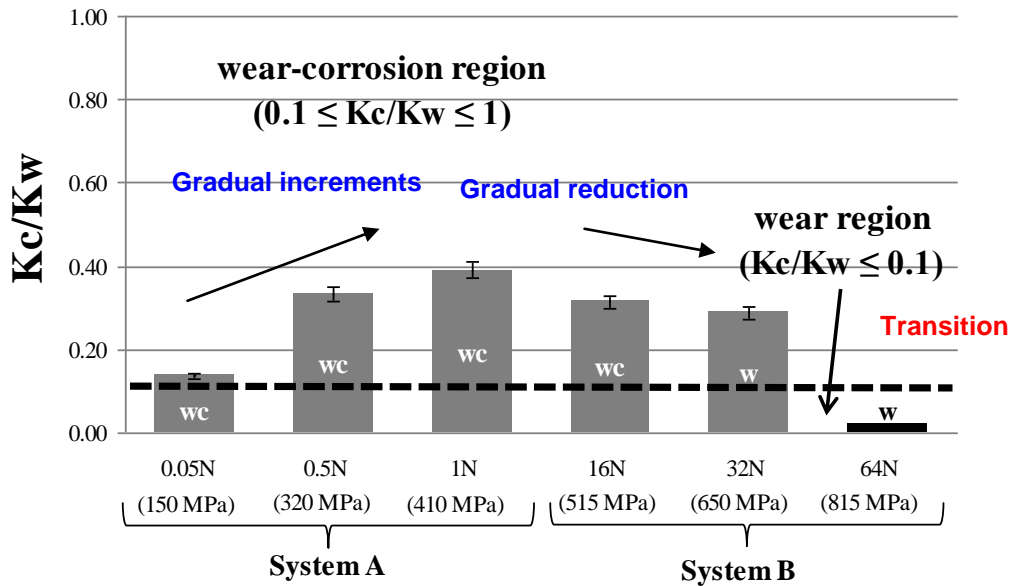
7 A point of particular interest in evaluating tribocorrosion are the synergistic interactions  
 8 between wear and corrosion, as they will affect the tribological mechanisms and could have a  
 9 significant influence on the amount of material loss. Stack et al [9, 13] determined that the ratio  
 10  $K_c/K_w$  of the chemical wear ( $K_c$ ) and mechanical wear ( $K_w$ ) provides a criterion for the  
 11 magnitude of this synergism and the ensuing dominant regime present in a tribocorrosion  
 12 system. The value of the “synergism” ratio is connected to the dominant degradation  
 13 mechanism as follows [13]:

<b>Synergism Ratio Value</b>	<b>Degradation Mechanism</b>
$K_c/K_w \leq 0.1$	Wear
$0.1 < K_c/K_w < 1$	wear-corrosion
$1 < K_c/K_w \leq 10$	corrosion-wear
$K_c/K_w > 10$	Corrosion

15  
 16 The values of  $K_c/K_w$  for Systems A and B are given in Table 5 and shown graphically  
 17 in Figure 11 as a function of load. In System A, the synergism ratio, lies in the range of  $0.1 <$   
 18  $K_c/K_w < 1$  for all loads, indicating the mass loss mechanism is a wear dominated corrosion  
 19 mechanism (wear-corrosion). In System B, a wear corrosion mechanism also dominates for the  
 20 first two loads. Then there is a transition to a wear dominated degradation mechanism at the  
 21 highest load. It is of interest that the synergism ratio increases gradually with load for System  
 22 A, but decreases with load for System B, suggesting that there is a contact stress which  
 23 maximizes synergism and that mechanical wear can dominate at both at low and high loads.  
 24 The latter is understandable because the corrosion rate is limited by its kinetics whereas the  
 25 mechanical wear can continue to increase with load. In particular this transition from wear-  
 26 corrosion to wear dominated regime is important because it may lead to the destruction of a

1 biotribolayer that is thought to increase the wear and corrosion resistance of CoCrMo alloys  
 2 Wimmer 2009 [14].

3



4

5

**Figure 11** – Synergistic interactions for each load of two systems. Grey bar: wear-6  
 corrosion regime (wc) Black bar: wear regime (w). 7

8

9 The two systems may also be compared with respect to their wear factors (Table 6).  
 10 The wear factors for System A are on average 31 times those for System B, suggesting that the  
 11 dominant wear mechanism is different in the two systems, perhaps due to the presence of  
 12 proteins in System B. However, other factors, such as differences in motion, contact stress, and  
 13 debris egress may also be significant. Perhaps a more fundamental comparison of the two  
 14 systems may be made by considering the total wear as a function of the total or accumulated  
 15 dissipated energy (Fouvry 2003 [23], Ramalho 2006 [24]), obtained by integrating the  
 16 frictional force over the sliding distance. The wear versus accumulated dissipated energy  
 17 curves downward for System A (Fig. 12(a)) but is fairly linear for System B (Fig. 12 (b)),  
 18 suggesting that in System A there is a mechanism rendering material removal less efficient at  
 19 the highest load. A possibility is that wear particles remaining within the wear area protect the  
 20 surface, either by re-adhering to it or acting as mini ball bearings. The average slope for

1 System A is 17 times that for System B, which lower than the corresponding ratio for the wear  
 2 factors (31), suggesting that the dissipated energy offers a somewhat better basis for  
 3 comparison of the two systems.

4 The comparison of results for tribocorrosion tests can be difficult, even for tests  
 5 following similar protocols. Thus, Mischler et al [22] conducted a multicenter study with seven  
 6 laboratories in Europe that entailed a prescribed protocol to assure similar conditions with the  
 7 tribometers, materials, environment, operating variables, surface cleaning, and electrochemical  
 8 measurements. It was found that no clear correlation existed between any single parameters  
 9 and the measured wear rates, but that the current during sliding was closely related to and  
 10 increased with the wear track area. Consistent with this finding, System A has greater wear  
 11 track area and corrosion current than System B, but the difference in electrolytes is a  
 12 confounding factor.

13

14

Table 6. Wear factors for Systems A and B

	<b>Normal load</b>	<b>k – Wear Coefficient (based on <math>K_{wc}</math>)</b>	<b>k – Wear Coefficient (based on <math>K_w</math>)</b>
<b>System A</b>	<b>0.05N</b>	0.0908	0.1042
	<b>0.5N</b>	0.5671	0.4252
	<b>1N</b>	0.3940	0.2832
<b>System B</b>	<b>16N</b>	0.0105	0.0080
	<b>32N</b>	0.0086	0.0066
	<b>64N</b>	0.0111	0.0114

15

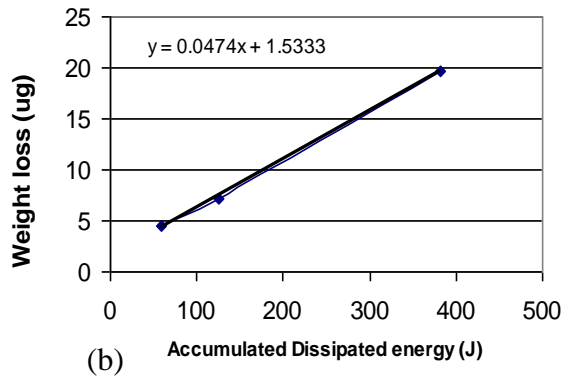
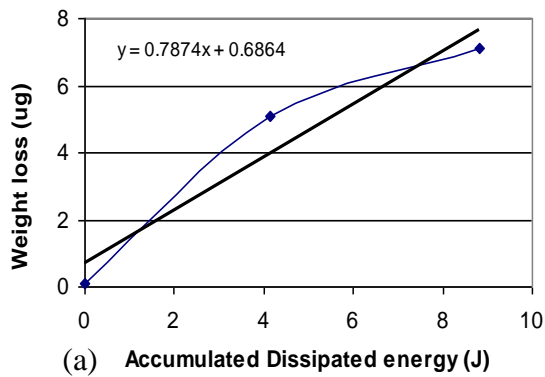


**Figure 12** – The evolution of weight loss as a function of dissipation energy for system A and System B.

## 4.2 Limitations

Because one of the objectives of this study was to compare a conventional test configuration as used by previous researchers with a test configuration geared to hip bearing applications, there were multiple test conditions that were simultaneously different between the two configurations, making it impossible to deconvolute the effect of each variable. Thus, the difference in motions, the lubricants, loads, and contact stresses were different in the two systems, so determining what was the effect of each of these variables when comparing the two systems was not possible. Also, although both tests were conducted under potentiostatic control at -0.345 V versus SCE, there was a possibility of a slight shift from this value [19, 22] during the tribocorrosion tests due to the tribochemical events at the surfaces. In using Faraday's law for the estimation of the mass  $K_c$  due to corrosion, the value  $n = 2$  was used, whereas the true value lies somewhere between 2 ( $\text{Co} \rightarrow \text{Co(II)}$ ) and 3 ( $\text{Cr} \rightarrow \text{Cr(III)}$ ). In addition, Pontiaux et al [19], highlighted the possible electrochemical interaction between worn and unworn area during the sliding, leading to the presence of galvanic couple that may impact corrosion processes.

## 5. Conclusions

The tribocorrosion behavior of a low-carbon CoCrMo alloy used for hip bearing applications was evaluated using two distinct tribometer configurations. In the first

1 configuration, “System A”, a linearly reciprocating alumina ball slid against the metal flat  
2 immersed in a phosphate buffer solution (PBS). In the second configuration, “System B”, the  
3 flat end of a cylindrical metal pin was pressed against an alumina ball that oscillated  
4 rotationally, using bovine calf serum (BCS) as the lubricant and electrolyte. System B was  
5 custom-built to more closely emulate *in vivo* conditions. The following conclusions were  
6 drawn:

- 7 • The tribocorrosion behavior of the CoCrMo alloy is influenced by the test system and  
8 required to be considered while interpreting the result.
- 9 • It was more favorable in System B, which was closer to *in vivo* conditions. Thus,  
10 comparing System B to System A:
  - 11 ○ The electrochemical impedance after sliding increased, whereas it decreased in  
12 System A.
  - 13 ○ The polarization resistance increased, rather than decreased as in System A,  
14 indicating a protective effect.
  - 15 ○ The friction coefficient in System B was lower than that in System A  
16 (approximately half in the case of highest load 1N and 64N).
  - 17 ○ The wear factor and energy dissipation per unit mass loss were over an order of  
18 magnitude lower in System B than A.
- 19 • Except at the normal highest load, the dominant mass loss mechanism was wear-  
20 corrosion, suggesting marked synergism between wear and corrosion. At the highest load,  
21 64 N in System B, the dominant mechanism was mechanical wear. Thus, there is a  
22 transition from wear-corrosion to mechanical wear somewhere between 32 and 64 N.
- 23 • The more favorable tribocorrosion behavior of the alloy in System B despite the higher  
24 contact stresses may stem from the proteins in the electrolyte lubricant providing  
25 boundary lubrication and assisting in the formation of a biotribolayer (Wimmer  
26 2010[14]). Other factors include less direct exposure of the worn area to the electrolyte.
- 27 • The results for System B suggest that the dominant mass loss mechanism in metal-on-  
28 metal bearings is wear-corrosion.
- 29 • The notable differences between the two systems indicate that emulating key aspects of  
30 the *in vivo* conditions is important.

1  
2  
3  
4  
5  
6  
7  
8  
9  
10  
11  
12  
13  
14  
15  
16  
17  
18  
19  
20  
21  
22  
23  
24  
25  
26  
27

Further work is required to identify all the key factors impacting the tribocorrosion of CoCrMo in the context of clinical applications. The identification of these factors may allow the formulation of a simplified, canonical tribocorrosion test that embodies the necessary aspects to evaluate alloys for hip bearings. An extensive study is planned to address such issues.

**Acknowledgements**

This study was funded by Luso-American Foundation (FLAD) grant in Portugal and NIH RC2 (1RC2AR058993-01) grant in Chicago. A special thanks to Prof. R Urban and Ms. D. Hall for assistance in SEM characterization. Acknowledgments also go to Dr. Thomas Pandorf of Ceramtech, Plochingen, Germany for providing ceramic heads.

**References**

[1] M.a.M.W.R.-. MMWR, Prevalence and Most Common Causes of Disability Among Adults — United States, 2005, in, Department of health and human services, Centers for Disease Control and Prevention, 2009.

[2] J.J. Jacobs, A.K. Skipor, L.M. Patterson, N.J. Hallab, W.G. Paprosky, J. Black, J.O. Galante, Metal Release in Patients Who Have Had a Primary Total Hip Arthroplasty. A Prospective, Controlled, Longitudinal Study, *J Bone Joint Surg Am*, 80 (1998) 1447-1458.

[3] P.F. Doorn, P.A. Campbell, J. Worrall, P.D. Benya, H.A. McKellop, H.C. Amstutz, Metal wear particle characterization from metal on metal total hip replacements: Transmission electron microscopy study of periprosthetic tissues and isolated particles, *Journal of Biomedical Materials Research*, 42 (1998) 103-111.

[4] E.F. DiCarlo, P.G. Bullough, The biologic responses to orthopedic implants and their wear debris, *Clinical Materials*, 9 (1992) 235-260.

[5] N. Hallab, K. Merritt, J.J. Jacobs, Metal Sensitivity in Patients with Orthopaedic Implants, *J Bone Joint Surg Am*, 83 (2001) 428-.

- 1 [6] Y. Yan, et al., Biotribocorrosion an appraisal of the time dependence of wear and corrosion  
2 interactions: I. The role of corrosion, *Journal of Physics D: Applied Physics*, 39 (2006) 3200.
- 3 [7] A.Navelle. Yu Yan , D. Dowson, Tribo-corrosion properties of cobalt-based medical  
4 implant alloys in simulated biological environments, *Wear*, 263 (2007) 1105–1111.
- 5 [8] T. Hanawa, S. Hiromoto, K. Asami, Characterization of the surface oxide film of a Co-Cr-  
6 Mo alloy after being located in quasi-biological environments using XPS, *Applied Surface*  
7 *Science*, 183 (2001) 68-75.
- 8 [9] M.M. Stack, N. Pungwiwat, Erosion-corrosion mapping of Fe in aqueous slurries: some  
9 views on a new rationale for defining the erosion-corrosion interaction, *Wear*, 256 (2004) 565-  
10 576.
- 11 [10] R.I. Trezona, D.N. Allsopp, I.M. Hutchings, Transitions between two-body and three-  
12 body abrasive wear: influence of test conditions in the microscale abrasive wear test, *Wear*,  
13 225-229 (1999) 205-214.
- 14 [11] K. Adachi, I.M. Hutchings, Wear-mode mapping for the micro-scale abrasion test, *Wear*,  
15 255 (2003) 23-29.
- 16 [12] J. Jiang, M.M. Stack, A. Neville, Modelling the tribo-corrosion interaction in aqueous  
17 sliding conditions, *Tribology International*, 35 (2002) 669-679.
- 18 [13] M.M. Stack, G.H. Abdulrahman, Mapping erosion-corrosion of carbon steel in oil  
19 exploration conditions: Some new approaches to characterizing mechanisms and synergies,  
20 *Tribology International*, 43 (2010) 1268–1277.
- 21 [14] M.A. Wimmer, A. Fischer, R. Büscher, R. Pourzal, C. Sprecher, R. Hauert, J.J. Jacobs,  
22 Wear mechanisms in metal-on-metal bearings: The importance of tribochemical reaction  
23 layers, *Journal of Orthopaedic Research*, 28 (2010) 436-443.
- 24 [15] D. Landolt, S. Mischler, M. Stemp, Electrochemical methods in tribocorrosion: a critical  
25 appraisal, *Electrochimica Acta*, 46 (2001) 3913-3929.
- 26 [16] Buscher. R, Tager G, Dudzinski W, et al, Subsurface Microstructure of metal-on-metal  
27 hip joints and its relationship to wear particles generation, *J. Biomed Material Res Part B: Appl*  
28 *Biomater* 72B: 206-214, 200
- 29 [17] Yoshida. H. et al. Three-dimensional hip contact area and pressure distribution during  
30 activities of daily living, *Journal of Biomechanics*, 39 (2006) 1996-2004.
- 31 [18] <http://www.alleghenytechnologies.com/allvac/pages/Nickel/UNSR31537.htm>



- 1 [19] Ponthiaux. P., Wenger. F., Drees. D., Celis. J.P. Wear, Vol. No. 256, 2004, pp 459-468.
- 2 [20] A.W.E. Hodgson, S. Kurz, S. Virtanen, V. Fervel, C.O.A. Olsson, S. Mischler, Passive  
3 and transpassive behaviour of CoCrMo in simulated biological solutions, Electrochimica Acta,  
4 49 (2004) 2167-2178
- 5 [21] A.W.E.H. S. Kurz, S. Virtanen, V. Fervel, S. Mischler, Corrosion characterization of  
6 passive films on CoCrMo with electrochemical techniques in saline and simulated biological  
7 solutions, European Cells and Materials, Vol. 3. Suppl. 1 (2002) 26-27.
- 8 [22] S. Mischler, Triboelectrochemical techniques and interpretation methods in  
9 tribocorrosion: A comparative evaluation, Tribology International, Volume 41, Issue 7, July  
10 2008, Pages 573-583
- 11 [23] S Fouvry, T. Liskiewicz , P. Kapsa,S. Hannel, E. Sauger. An energy description of wear  
12 mechanisms and its applications to oscillating sliding contacts. Wear. 2003;255(1-6):287-298.
- 13 [24] A. Ramalho , JC Miranda , The relationship between wear and dissipated energy in sliding  
14 systems. Wear. 2006;260(4-5):361-367.

15

16 **List of tables:**

17 Table 1 - Source, Rockwell hardness, and elemental composition of the low-carbon wrought  
18 CoCrMo alloy used in this study.

19 Table 2 - Chemical composition of PBS solution, used in System A.

20 Table 3 - Chemical composition of BCS solution, used in System B.

21 Table 4 – Test conditions and a comparison between systems A and B.

22 Table 5 - Wear-corrosion volume loss for the highest normal loads of both systems.

23 Table 6 - Wear factors for Systems A and B.

24

25 **List of figures:**

26 Figure 1 - Schematic diagram for the three-element Randles equivalent circuit used to  
27 determine the polarization resistance ( $R_p$ ).  $R_{sol}$  represents the solution resistance and  $C_{dl}$   
28 represents the double layer capacitance.

29 Figure 2 - Polarization curve of low carbon CoCrMo alloy in PBS and BCS solutions. Potential  
30 range from -0.8 to 1.8V, scan rate of 1mV/sec.

1 Figure 3 - Depiction of the conventional CETR tribometer for System A. (a) Tribometer set-up.  
2 (b) Test area. (c) Top view of the test area.

3 Figure 4 - Depiction of the pin-on-ball custom built tribometer, System B, used in this study.  
4 (a) The tribometer set-up. (b) The test area. (c) Top view of the test area.

5 Figure 5 - Evolution of the current and the friction coefficient during a 30 minute sliding run at  
6 (a) 1N in PBS solution (System A) and at (b) 64N in BCS solution (System B). Dotted line (Z-  
7 Z') shows zero current.

8 Figure 6 - Bode plot from electrochemical impedance spectroscopy measurements for (a) 1N in  
9 PBS solution and for (b) 64N in BCS solution, System A and B, respectively.

10 Figure 7 - Polarization resistance before and after sliding at the highest normal load in (a)  
11 System A and in (b) System B.

12 Figure 8 - 3-dimensional image of the wear scar using Zygo Microscope for (a) System A and  
13 (b) System B, with 1N and 64N, respectively.

14 Figure 9 - SEM micrographs of the wear scars on the CoCrMo surface for System A (left side,  
15 (a) and (b)) at 1N and for System B (right side, (c) and (d)) at 64N. (e) Typical EDS spectrum  
16 for pits and passive film on the surface.

17 Figure 10 - Total weight loss distribution for (a) System A and (b) System B.

18 Figure 11 - Synergistic interactions for each load of two systems. Grey bar: wear-corrosion  
19 regime (wc); Black bar: wear regime (w).

20 Figure 12 - The evolution of weight loss as a function of dissipation energy for system A and  
21 System B.

22  
23 Tribocorrosion Behavior of CoCrMo Alloy for Hip Prostheses as a function of Loads: A  
24 Comparison between Two Testing Systems  
25